The Astrophysical Journal, 815:119 (8pp), 2015 December 20 doi:10.1088/0004-637X/815/2/119

NEW MODELING OF GALACTIC PROTON MODULATION DURING THE MINIMUM OF SOLAR CYCLE 23/24

Etienne E. Vos and Marius S. Potgieter
Centre for Space Research, North-West University, 2520 Potchefstroom, South Africa; etienne.eevos@gmail.com, marius.potgieter@nwu.ac.za
Received 2015 October 12; accepted 2015 November 7; published 2015 December 16

ABSTRACT

During the recent prolonged solar minimum of cycle 23/24, the *PAMELA* detector measured 27-day averaged Galactic proton energy spectra over the energy range that is important for solar modulation. By comparing these spectra to computed spectra from a three-dimensional model that contains all of the important heliospheric modulation processes, the recent minimum can be studied in detail from a modulation perspective. This was done by setting up a realistic heliosphere in the model, and reproducing a representative selection of seven intermittent *PAMELA* spectra, separated by approximately six months, from 2006 July to 2009 December. Additionally, a new very local interstellar proton spectrum was constructed using measurements below 600 MeV from *Voyager 1*, taken beyond the heliopause, combined with *PAMELA* and *AMS-02* measurements above 30 GeV at the Earth. As a result of the extreme minimum modulation conditions that governed the recent solar minimum, the highest ever Galactic cosmic ray spectrum at Earth was observed by *PAMELA* at the end of 2009. It was found that, apart from the self-consistent changes in the heliospheric current sheet and the heliospheric magnetic field over time, additional increases in the mean free paths during this period were required below ∼4 GV in order to reproduce the intensities observed by *PAMELA*.

Key words: cosmic rays – stars: activity – Sun: heliosphere

1. INTRODUCTION

With the availability of accurate proton energy spectra measured by *PAMELA* during the recent unusual minimum of 2009 (Adriani et al. 2013), this solar minimum period can be studied in detail with regard to how the proton energy spectrum developed. Potgieter et al. (2014) conducted a similar study, aiming to uncover the extent to which various modulation processes contributed to the high intensities observed by *PAMELA*, as well as to prove the interplay that exists among these processes. These authors also studied the modulation of Galactic electrons between 2006 and 2009, and concluded that even though the solar minimum of cycle 23/24 seemed to have been diffusion-dominated, all modulation processes still played important roles, including gradient, curvature, and current-sheet drifts.

A major development that influences modeling results are the recent Galactic cosmic-ray (GCR) observations made by *Voyager 1* in the very local interstellar medium (LISM) after it crossed the heliopause (HP) in 2012 August (Stone et al. 2013). Since these observations are largely unaffected by solar modulation, they enable us to adjust the proton very local insterstellar spectrum (LIS) between 3 and 600 MeV accordingly. It has also been shown that the amount of modulation experienced by GCRs above 30–50 GeV becomes negligible, so that *PAMELA* and *AMS-02* observations at the Earth in this energy range can be considered as accurate intensity levels for the very LISM.

A newly constructed very LIS for protons, based on the above mentioned observations, is presented here, and used as an input spectrum for modeling solar modulation. The modulation model used here also utilizes a modification to the heliospheric magnetic field (HMF) as proposed by Smith & Bieber (1991).

This study aims to broaden the work of Potgieter et al. (2014) by reproducing *PAMELA* spectra during the recent solar minimum of cycle 23/24 over smaller intervals, while also taking into account *Voyager* measurements at different radial distances and spatial gradients in the inner heliosphere. These improvements resulted in quantitative changes to the diffusion coefficients (DCs) compared with Potgieter et al. (2014).

The results of a detailed study of the *Voyager* radial profiles and the radial and latitudinal gradients between *PAMELA* and the position of *Ulysses* will be presented in an upcoming publication.

2. A NEW LOCAL INTERSTELLAR PROTON SPECTRUM

Many attempts have been made to obtain reliable LIS estimates for protons in the energy range important for solar modulation. Only with the recent availability of in situ measurements by *Voyager 1* from beyond the HP this has become possible.

Figure 1 gives the proton very LIS used in this study. *Voyager 1* observations (diamonds) below ∼600 MeV were used to set the absolute value of the spectrum beyond the HP (Stone et al. 2013; Webber & McDonald 2013), while *PAMELA* and *AMS-02* measurements (Adriani et al. 2013; Aguilar et al. 2015) were used to normalize the very LIS above 30 GeV, where solar modulation is considered negligible (shaded band). GALPROP solutions (see, e.g., Moskalenko et al. 2002) were used as a guide between 600 MeV and 30 GeV. The top and bottom panels of Figure 1 give the differential intensity and corresponding spectral index, respectively.

The spectral index from the top panel of Figure 1 remains mostly constant at −2.78 between 30 and 50 GeV, and corresponds to that reported for *PAMELA* and *AMS-02*. Below 10 MeV the shape levels off to a fairly steady index of 0.12. The difference between the LIS and the *PAMELA* and *AMS-02* observations below 30 GeV is indicative of solar modulation.

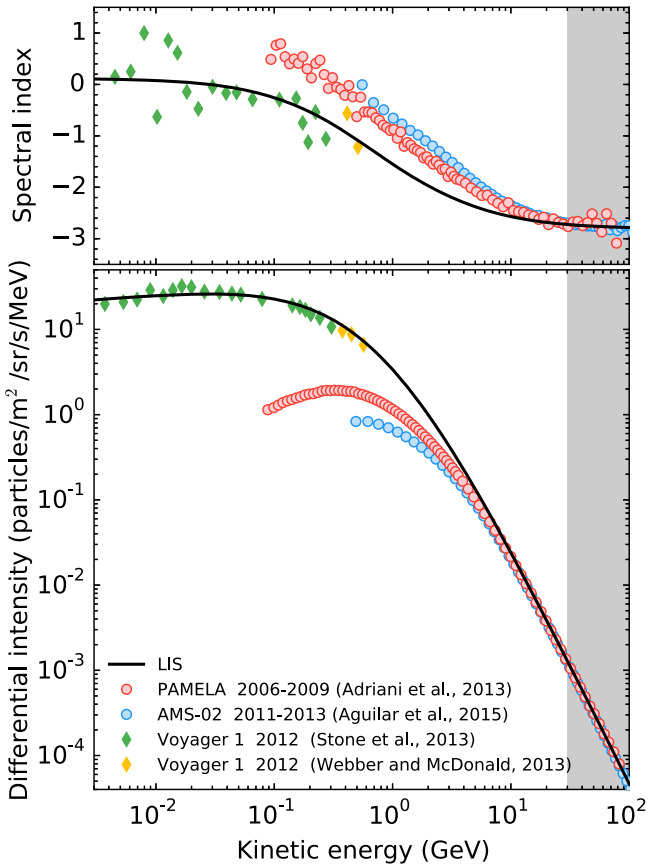

Figure 1. Newly constructed proton very LIS used in this study (black line). *PAMELA*, *AMS-02*, and *Voyager 1* observations (colored symbols) were used to obtain this very LIS. Differential intensity is given in the bottom panel with the corresponding spectral index shown in the top panel. The very LIS is normalized to observations above 30 GeV (gray band).

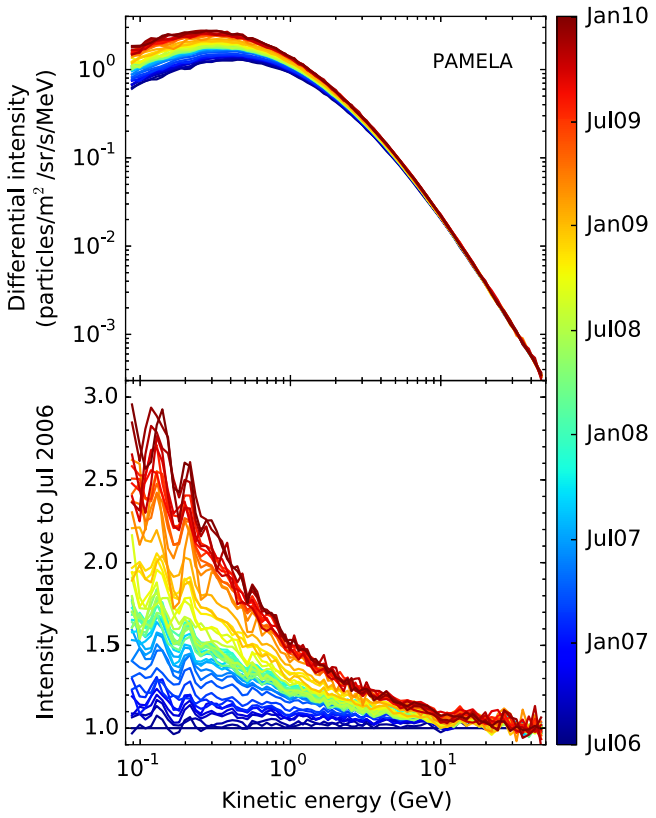

Figure 2. Top panel: *PAMELA* 27-day averaged proton energy spectra (Adriani et al. 2013), observed between 2006 July (blue) and the beginning of 2010 January (red). Bottom panel: consecutive ratios of the *PAMELA* energy spectra in the top panel, relative to 2006 July. The spread between the blue and red spectra represents modulation-dependent changes over the considered time period.

This very LIS is given by

$$j_{\rm LIS} = 2.70\,\frac{E^{1.12}}{\beta^2}\left(\frac{E+0.67}{1.67}\right)^{-3.93}, \qquad (1)$$

where E is the kinetic energy in GeV, $\beta = v/c$ the ratio of particle speed relative to the speed of light, and $j_{\rm LIS} = P^2 f$ is the differential intensity given in units of particles $\mathrm{m^{-2}\,s^{-1}\,sr^{-1}\,MeV^{-1}}$, with P as the rigidity in GV and f as the GCR distribution function.

In the model, the very LIS is specified at the HP, taken at 122 AU. Modulation beyond the HP is not considered here; see, e.g., Strauss et al. (2013) and Luo et al. (2015).

3. THE *PAMELA* PROTON SPECTRA

The top panel of Figure 2 gives an overview of the proton energy spectra measured by *PAMELA*, averaged over Carrington rotations, from 2006 July to the end of 2009 (Adriani et al. 2013). The bottom panel gives the intensity ratios relative to 2006 July. The change in color represent the development with time, as indicated by the colorbar, with 2006 July given in blue and the beginning of 2010 January given in red.

As expected, the lowest energy GCRs, being the most responsive to changes in modulation conditions, have undergone the largest increase throughout this minimum period—by a factor of ∼3 around 100 MeV. At higher energies, this increase becomes less pronounced, with intensity variations below 20% for GCRs above 10 GeV, from the bottom panel of Figure 2. The assumption that GCR modulation can be neglected above 30 GeV is supported by the fact that ratios in this energy range show very little to no observable changes; see also Strauss & Potgieter (2014a).

As a result of solar activity reaching extremely low levels during the recent prolonged minimum of solar cycle 23/24 (e.g., Mewaldt et al. 2010; Kane 2011) *PAMELA* measured the highest ever GCR spectrum at Earth at the end of 2009. This spectrum is shown in Figure 3 by the solid blue circles, and clearly exceeds proton spectra from other experiments taken at different times in the solar cycle (see the legend). *PAMELA* observations also show a clear consensus with other experiments with regard to normalization above 30 GeV.

The blue, orange, and red bands in Figure 3 indicate what are considered to be minimum, moderate, and maximum modulation regimes, respectively, classified according to the heliospheric current-sheet (HCS) tilt angles, which is a very good proxy for solar activity and the subsequent GCR modulation. Minimum modulation usually occurs for tilt angles below ∼15°, while maximum modulation occurs for tilt angles larger than ∼50°, with moderate modulation in between. See, e.g., Strauss & Potgieter (2014b) for a comparison of $A < 0$ and $A > 0$ spectra observed during solar minimum activity.

The primary objective of this work is to reproduce intermittent *PAMELA* proton spectra measured between 2006 July and 2009 December, using a three-dimensional (3D) modulation model, and utilizing what is known about

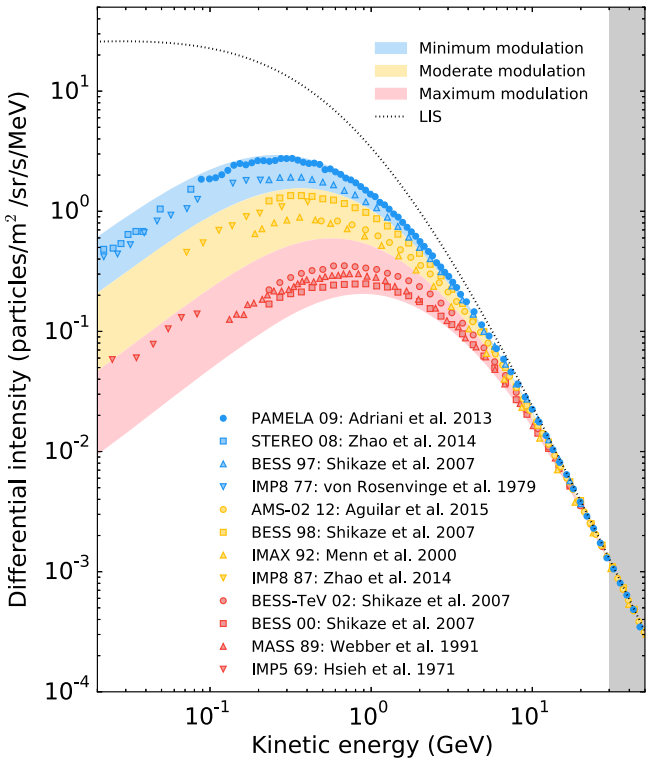

Figure 3. Proton spectrum measured by *PAMELA* at the end of 2009 (solid blue circles), recognized as being the highest spectrum ever recorded at the Earth, is compared to spectra from other experiments at different times in the solar cycle. Blue, orange, and red bands show approximate regimes for minimum, moderate, and maximum heliospheric modulation, respectively. The gray band is where modulation is considered negligible.

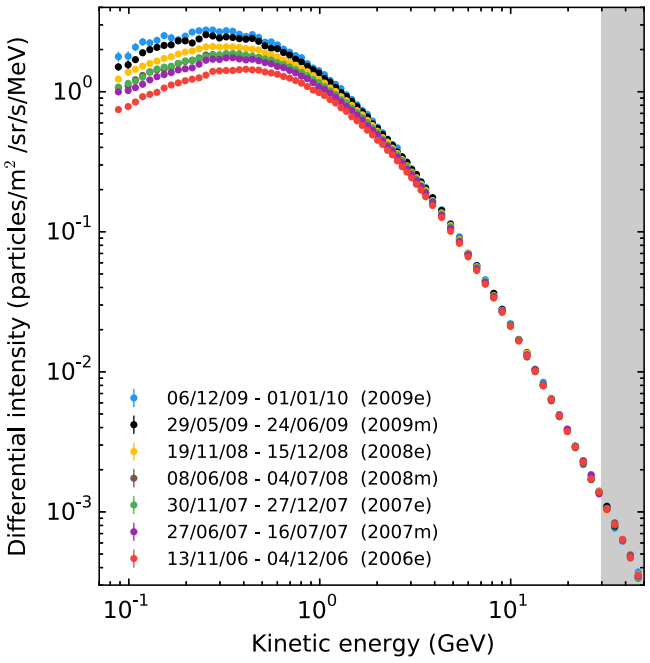

Figure 4. Selection of seven 27-day averaged proton spectra measured by *PAMELA*. These spectra, taken at the end of each semester from 2006 November to 2009 December, serve as a representative sample of how the proton spectrum changed over time.

modulation conditions in the heliosphere. A representative selection of 27-day averaged *PAMELA* proton spectra, taken at the end of each semester, is shown in Figure 4. The time-periods of these spectra are given in the legend, and are from hereon referred to as the 2006e, 2007m, 2007e, 2008m, 2008e, 2009m, 2009e spectra, where the "m" and "e" suffixes denote the middle and end of each year, respectively.

4. MODELING THE *PAMELA* PROTON SPECTRA

A full 3D modulation model is used to compute differential intensities of GCR protons at the Earth, and is based on the numerical solution of the heliospheric transport equation from Parker (1965):

$$\frac{\partial f}{\partial t} = -\left(\boldsymbol{V} + \langle v_{\rm D}\rangle\right)\cdot\nabla f + \nabla\cdot\left(\boldsymbol{K}_s\cdot\nabla f\right) + \frac{1}{3}(\nabla\cdot\boldsymbol{V})\frac{\partial f}{\partial \ln P}, \quad (2)$$

with f as the GCR distribution function, and t as the time, where we study the steady-state case $\partial f/\partial t = 0$, for modulation during solar minimum when modulation parameters change gradually. The terms on the right-hand side, respectively, represent convection, with V as the solar wind (SW) velocity; averaged particle drift velocity $\langle v_{\rm D}\rangle$ caused by gradients, curvatures, and HCS drifts in the global HMF; diffusion, with $\boldsymbol{K}_S$ as the symmetric diffusion tensor; adiabatic cooling, with P as the rigidity.

The numerical model used in this study is further described in detail by Potgieter et al. (2014, 2015). The modulation parameters as modeled are discussed below. For a comprehensive review of the underlying theory, see Potgieter (2013).

4.1. Calculating the Intrinsic Parameters

When working with a steady-state modulation model, it is often a challenge to determine representative values for time-varying modulation parameters. The HCS tilt angle and the HMF at Earth changed pronouncedly over a four-year span prior to 2009. These time-dependent changes are accounted for by setting up realistic modulation conditions in the model that coincide with the 27-day averaged spectra given in Figure 4. Moving averages were used to approximate these conditions at the times when the selected spectra were observed.

Figure 5 gives the HCS tilt angle and HMF at Earth (top and bottom panels, respectively), along with moving averages (red lines and circles). The calculation of these averages is based on the time it takes for the tilt angles and the frozen-in HMF to travel from the Sun to the HP, as they are carried outward by the SW. These propagation times serve as a window over which preceding averages are calculated. The HCS is mostly confined to the ecliptic region during moderate to minimum solar activity (within an $\sim$30° latitudinal extent) and, therefore, remains in the slow SW region. Knowing the averaged SW speed in the slow SW region ($\sim$430 km s^{-1} upwind of the termination shock, TS), the propagation time for the tilt angle is calculated to be $\sim$16 months. For the HMF, both the slow and fast (750 km s^{-1}) SW regions are taken into account by means of a weighted moving average, where the weights are determined by the volume occupied by the different SW regions. Following this approach, the HMF's propagation time calculates to $\sim$10 months.

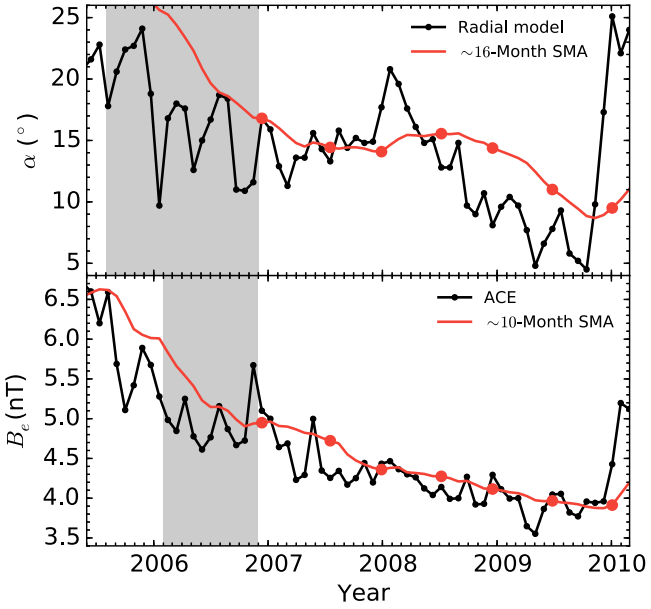

Figure 5. Top panel: tilt angle values, α, from the radial HCS model taken from http://wso.stanford.edu (black line), along with a ~16-month moving average (red line). Bottom panel: heliospheric magnetic field magnitude at Earth (B_e) from http://omniweb.gsfc.nasa.gov, with a ~10-month moving average. Average values indicated by the red circles are used as representative values for preceding conditions. For illustrative purposes, the different averaging windows used for calculating the 2006e average α and B_e are given by the shaded bands.

In addition to these solar activity variables, the position of the TS also varies with time due to the dynamic nature of the heliosphere (e.g., Richardson & Wang 2011), which affects modulation intensities even at Earth (see, e.g., Manuel et al. 2014). All of these parameters have been accounted for in the model and are summarized in Table 1.

4.2. The Numerically Reproduced PAMELA Spectra

By also carefully adjusting the DCs as described in Section 5, the *PAMELA* spectra from Figure 4 were successfully reproduced. The 2006e measured and computed spectra in Figure 6 were used as a reference against which to compare how the spectrum developed during the rest of the solar minimum period. The reproduced *PAMELA* spectra between 2007 and 2009 are shown in Figure 7. *PAMELA* spectra from the previous semesters are given by the gray symbols.

The model reproduces the behavior of GCRs above 30 GeV, where heliospheric modulation becomes negligible. Below 100 MeV the modulated spectra bend into the characteristic E^1 slope as a result of adiabatic deceleration from the expanding SW (see also Heber & Potgieter 2006). For protons, this process becomes dominant at non-relativistic energies (below 100–200 MeV). GCRs below these energies experience a noticeable amount of modulation, even at large radial distances, illustrating the effectiveness of this modulation process.

From Figure 6, it follows that the proton spectrum at Earth in 2006 November had a peak intensity of 1.4 particles $m^{-2}\,s^{-1}\,sr^{-1}\,MeV^{-1}$ at 400 MeV. The model shows how this peak shifts to lower energies when moving further out into the heliosphere—a phenomenon that is determined by the shape of the LIS and through the process of energy-losses (see, e.g., Moraal & Potgieter 1982). From Figures 6 and 7, it is clear that the proton spectrum became progressively softer from 2006 to 2009, reaching an intensity of 2.7 particles $m^{-2}\,s^{-1}\,sr^{-1}\,MeV^{-1}$ at the end of 2009, with an accompanying shift of the spectrum peak down to 270 MeV. Consequent predictions of intensity levels can be made for energies below 80 MeV, where *PAMELA* measurements are unavailable. At 10 MeV, 2006e intensities are estimated at ~0.09 particles $m^{-2}\,s^{-1}\,sr^{-1}\,MeV^{-1}$, and increased to ~0.3 particles $m^{-2}\,s^{-1}\,sr^{-1}\,MeV^{-1}$ at the end of 2009.

4.3. Intensity Ratios

Figure 8 shows the ratios of the consecutive reproduced spectra from Figure 7 relative to the 2006e reference spectrum in Figure 6, and gives a quantitative measure of the total variability. Good agreement between measurements and computed spectra is reflected in the fact that the computed spectra adheres to the constraints of the statistical errors from the observations.

At 10 MeV it is estimated that intensities in 2009e increased by a factor of 3.3 relative to 2006e. The largest semesterly increase of ~65% occured between 2008e and 2009m, likely due to the recovery of GCRs following the transient decrease during the first semester of 2008. Conversely, the sudden increase in tilt angle during 2008, and the corresponding solar activity, temporarily suppressed intensities, resulting in almost identical spectra for 2007e (green) and 2008m (brown). Since the HMF continued to decrease during 2008 (bottom panel of Figure 5), this transient effect experienced by GCRs is linked to current-sheet drifts and supports the presence of such a modulation mechanism during the recent solar minimum.

Figure 9 shows the modulation reduction factor (MRF) of the reproduced spectra, calculated by taking the ratio of the modulated spectra relative to the LIS. At high energies, the MRF approaches unity, indicating how the amount of modulation decreases with increasing energy. It follows that GCR protons experienced less than ~10% solar modulation above 30 GeV, similar to what was found by Strauss & Potgieter (2014a), who used a model based on stochastic differential equations (SDEs) in an independent study. Measurements above 30–50 GeV should therefore reflect astrophysical processes.

Energy ranges where the MRF is larger than 0.9, 0.5, and 0.1 are indicated by the gray shaded bands in Figure 9. Evidently, below 30 GeV, solar modulation effects become increasingly dominant. At the lower end of the spectrum (around 100 MeV), the MRF is already at ~0.03.

4.4. Proton Intensity Over Time

For a qualitative and quantitative understanding of the temporal development of the proton spectrum, Figure 10 shows the observed *PAMELA* intensities (solid lines) with statistical errors (shaded bands) in the 500 MeV–3 GeV energy range from mid-2006 to the end of 2009, as well as the model intensities at the same energies (dashed lines and filled circles), with the different energy ranges color-coded. Time-dependent modulation diminishes at higher energies, as seen in the comparatively smaller increases and variations toward 3 GeV.

During 2007, intensities increased gradually. In 2008, however, as a result of the sudden increase in the HCS tilt angle, proton intensities decreased notably across all energies and started recovering in the middle of 2008. During 2009,

Table 1
A Summary of the Intrinsic Modulation Parameters Used in Reproducing the *PAMELA* Spectra

Parameter	2006e	2007m	2007e	2008m	2008e	2009m	2009e
α (°)	16.80	14.43	14.08	15.56	14.38	11.01	9.50
B_e (nT)	4.95	4.72	4.36	4.27	4.11	3.97	3.91
r_{TS} (AU)	88.0	87.0	86.0	85.0	84.0	82.0	80.0

Note. Here α, B_e, and r_{TS} refer to the HCS tilt angle, the HMF at Earth, and the assumed radial distance at which the TS was located in the model, respectively. The HP is taken at 122 AU.

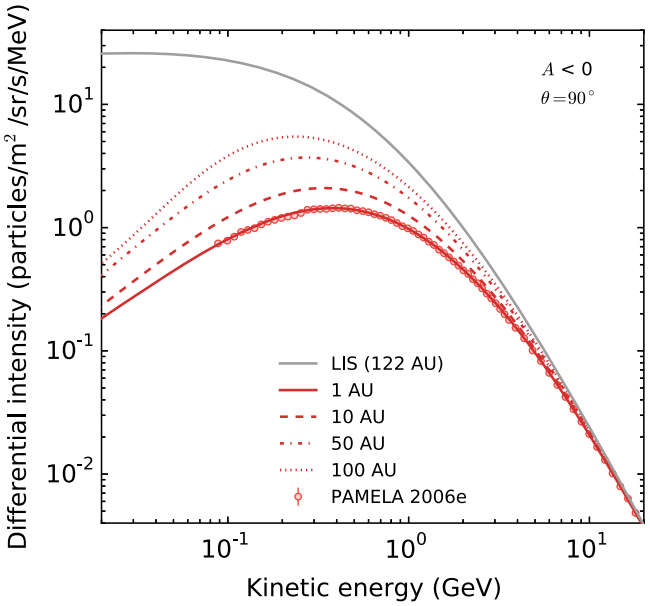

Figure 6. Reproduced and observed *PAMELA* 2006e spectrum, used as a reference spectrum for the development of the solar minimum up to the end of 2009. Computed spectra at 1, 10, 50, and 100 AU are given by the solid, dashed, dashed–dotted, and dotted lines, respectively, in the equatorial plane (i.e., $\theta = 90°$). The LIS from Figure 1 (gray line) is specified at 122 AU.

intensities increased more rapidly than during the previous two years, because of the continued decrease in solar activity.

Figure 11 shows the normalized *PAMELA* observations relative to 2006e (top panel). Apart from including time-dependent changes in α and B_e for reproducing the selected *PAMELA* spectra (Table 1), additional increases in the DCs were required below ~4 GV in order to reach measured intensity levels (middle panel). When the latter increases were excluded in the model, intensities were found to be ~75% smaller than *PAMELA* observations at 100 MeV (bottom panel). See also Potgieter et al. (2014).

5. RIGIDITY AND SPATIAL DEPENDENCE OF THE DCS

As the heliosphere approached solar minimum conditions, it can be inferred that the HMF became more structured in the years leading up to 2009 (e.g., McComas et al. 2008), which effectively reduced the amount of turbulence in the heliosphere and increased particle mean free paths (MFPs). These increases, combined with drifts, are expected to be responsible for the intensity increase observed across the greater part of the proton spectrum between 2006 and 2009. The numerical solutions given in Figures 6 and 7 were obtained by using a phenomonological diffusion approach that approximates QLT (e.g., Potgieter 2000; Shalchi 2009), while still adhering to constraints from recent studies.

Figure 12 shows the rigidity dependence of the parallel ($\lambda_\parallel$) and perpendicular ($\lambda_\perp$) MFPs, and the drift scale (λ_A) obtained after reproducing the 2006e to 2009e spectra. With the DCs related to the MFPs by $\kappa = \lambda(v/3)$, with v as the particle speed, the equation for diffusion parallel to the average background HMF is given by

$$\kappa_\parallel = \kappa_{\parallel 0}\, \beta\, F(r, \theta, \phi) G(P), \tag{3}$$

with

$$F(r, \theta, \phi) = \frac{B_0}{B}, \tag{4}$$

and

$$G(P) = \left(\frac{P}{P_0}\right)^a \left\{ \frac{\left(\frac{P}{P_0}\right)^c + \left(\frac{P_k}{P_0}\right)^c}{1 + \left(\frac{P_k}{P_0}\right)^c} \right\}^{\frac{b-a}{c}}, \tag{5}$$

where $\kappa_{\parallel 0}$ is a scaling constant in units of $\mathrm{cm^2\,s^{-1}}$, B is the magnetic field magnitude in nT, with β and P as discussed before. The variables a, b, c, and P_k determine the shape of the MFP rigidity dependence, which has the functional form of two combined power laws. The constants $B_0 = 1$ nT and $P_0 = 1$ GV are to keep F and G dimensionless. Most of the parameters in Equation (5) are given in Table 2.

The expression for the HMF, as modified by Smith & Bieber (1991) is

$$B = B_n \left(\frac{r_0}{r}\right)^2 \sqrt{1 + \tan\psi^2}, \tag{6}$$

with $r_0 = 1$ AU, and $\tan\psi$ as a function of radial distance (r) and polar angle (θ) given by

$$\tan\psi = \frac{\Omega(r - r_{sb})\sin\theta}{V(r, \theta)} - \frac{r\, V(r_{sb}, \theta)}{r_{sb}\, V(r, \theta)} \frac{B_T(r_{sb})}{B_R(r_{sb})}. \tag{7}$$

Here B_n is a normalization constant that assures the HMF has the value B_e at Earth, Ω is the angular velocity of the Sun, and V is the SW speed. With $r_\odot = 0.005$ AU as the solar radius, the value $r_{sb} = 10\, r_\odot$ and the ratio $B_T/B_R = 0.15$ are constants that determine the HMF modification.

For diffusion perpendicular to the magnetic field lines, a rigidity dependence similar to that of $\lambda_\parallel$ is assumed below 4 GV, while a slightly weaker dependence of $P^{1.58}$ is assumed above 4 GV. A distinction is made between the radial ($\kappa_{\perp r}$) and polar ($\kappa_{\perp\theta}$) diffusion directions, where the former and latter are scaled by 2% and 1% of the parallel diffusion respectively. This differs from what Potgieter et al. (2014) used and is in line with what is required from turbulence theory (see, e.g., Burger et al. 2000; Strauss et al. 2013, and Manuel et al. 2014). These

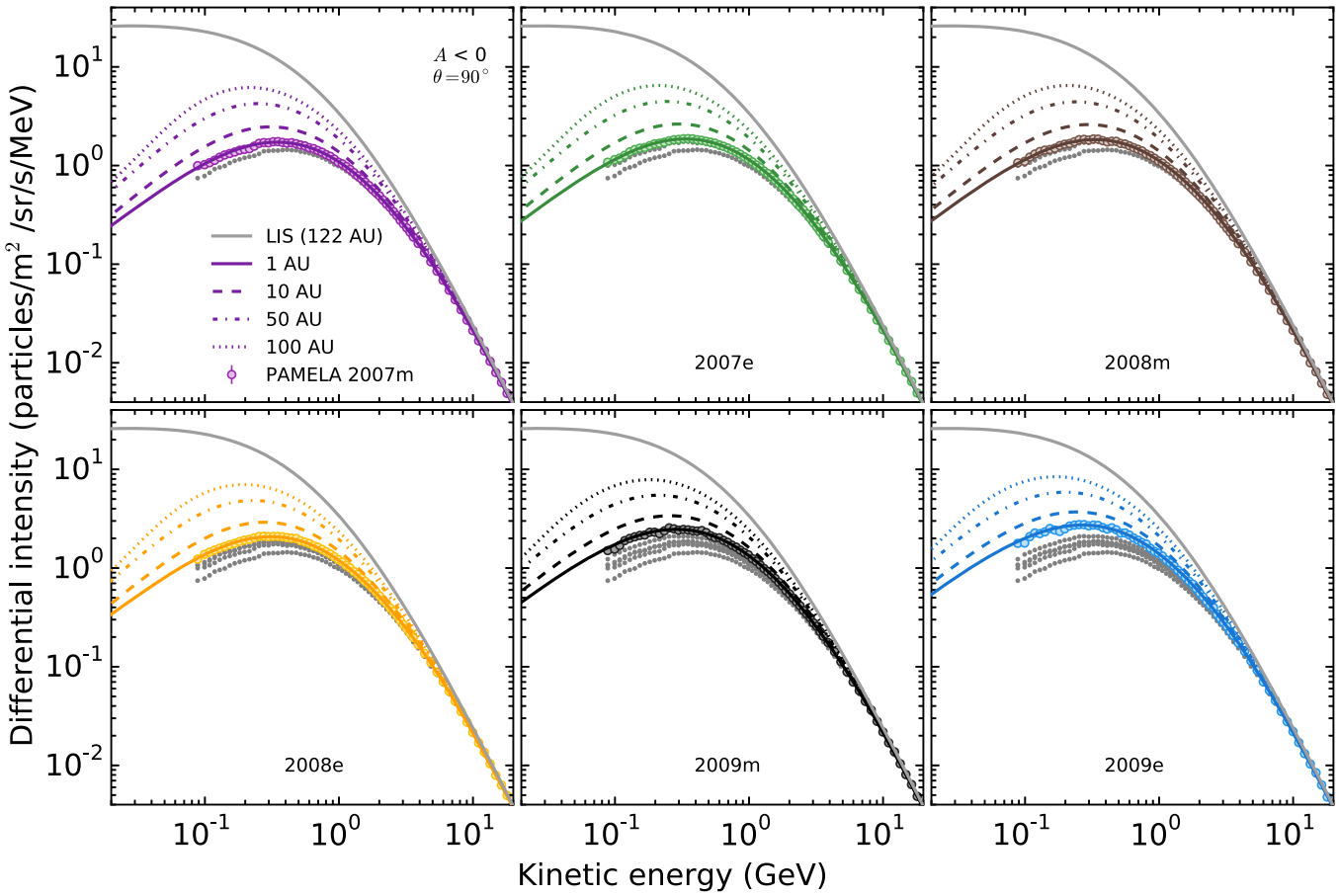

Figure 7. Similar to Figure 6, but for the reproduced and observed *PAMELA* spectra at the end of each semester, between 2007 and 2009. As a reference, the gray circles represent all the previously reproduced *PAMELA* spectra.

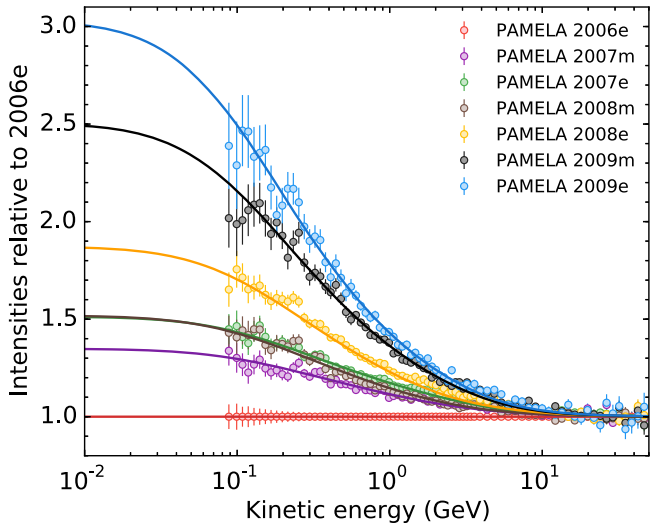

Figure 8. Ratios of consecutive computed (lines) and measured (symbols) proton spectra from Figure 7, relative to the 2006e reference spectrum in Figure 6.

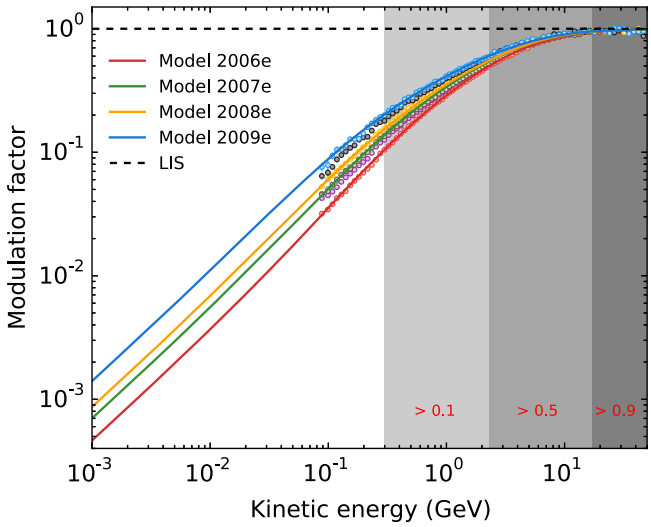

Figure 9. Modulation reduction factor for the reproduced spectra between 2006 November and 2009 December, calculated by taking the ratio of the modulated spectra to the appropriate LIS value.

coefficients are given by

$$\kappa_{\perp r} = 0.02\ \kappa_{\parallel 0}\ \beta\ F(r,\ \theta,\ \phi)G(P) \tag{8}$$

and

$$\kappa_{\perp\theta} = 0.01\ \kappa_{\parallel 0}\ \beta\ F(r,\ \theta,\ \phi)G(P)h_{\perp\theta}, \tag{9}$$

where

$$h_{\perp\theta} = A^{+} \mp A^{-} \tanh\left[8\left(\theta_A - 90^\circ \pm \theta_F\right)\right], \tag{10}$$

with $A^{\pm} = (3 \pm 1)/2$, $\theta_F = 35^\circ$, $\theta_A = \theta$ for $\theta \leqslant 90^\circ$ but $\theta_A = 180^\circ - \theta$ for $\theta > 90^\circ$. Equation (10) enhances $\kappa_{\perp\theta}$ in the polar regions as motivated by, e.g., Potgieter (2000).

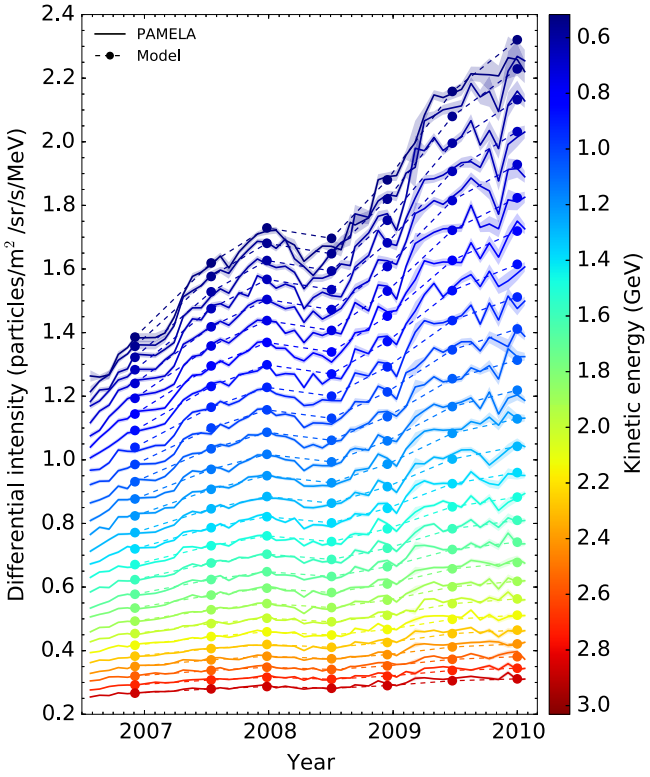

Figure 10. *PAMELA* proton intensities (solid lines), along with statistical errors (shaded bands) are compared to computed intensities (dashed lines and filled circles) over time. Different energies are represented by the range of colors according to the color bar on the right.

The rigidity and spatial dependence for the drift coefficient is given by

$$\kappa_A = \frac{\beta P}{3B} \frac{\left(\frac{P}{P_{A0}}\right)^2}{1 + \left(\frac{P}{P_{A0}}\right)^2}, \quad (11)$$

which reduces drifts below $P_{A0} = 0.55$ GV with respect to the weak scattering case (e.g., Ngobeni & Potgieter 2015). This is required to explain the small latitudinal gradients observed by *Ulysses* at low rigidities (Heber & Potgieter 2006; De Simone et al. 2011). Table 2 gives the values of the modulation variables obtained after reproducing the year-end spectra in Figures 6 and 7.

As a result of using different rigidity dependencies for $\kappa_\parallel$ and $\kappa_\perp$, as proposed by turbulence theory (e.g., Burger et al. 2000), some differences in the values for these coefficients exist when compared to a similar study from Raath et al. (2015). These differences are also ascribed to dissimilar parameters in the HMF modification.

The combined increases that were required for proton MFPs below ~4.0 GV resulted in a change in slope for the rigidity dependence from $P^{0.9}$ in 2006, to $P^{0.8}$ in 2009. This is a stronger dependence than the $P^{1/3}$ suggested by the random sweeping and damping turbulence models (see also Potgieter 2000). Above ~3.0 GV the rigidity slope gradually steepens to $P^{2.1}$, similar to the P^2 dependence found by Pei et al. (2010) following their QLT-based analysis of $\lambda_\parallel$.

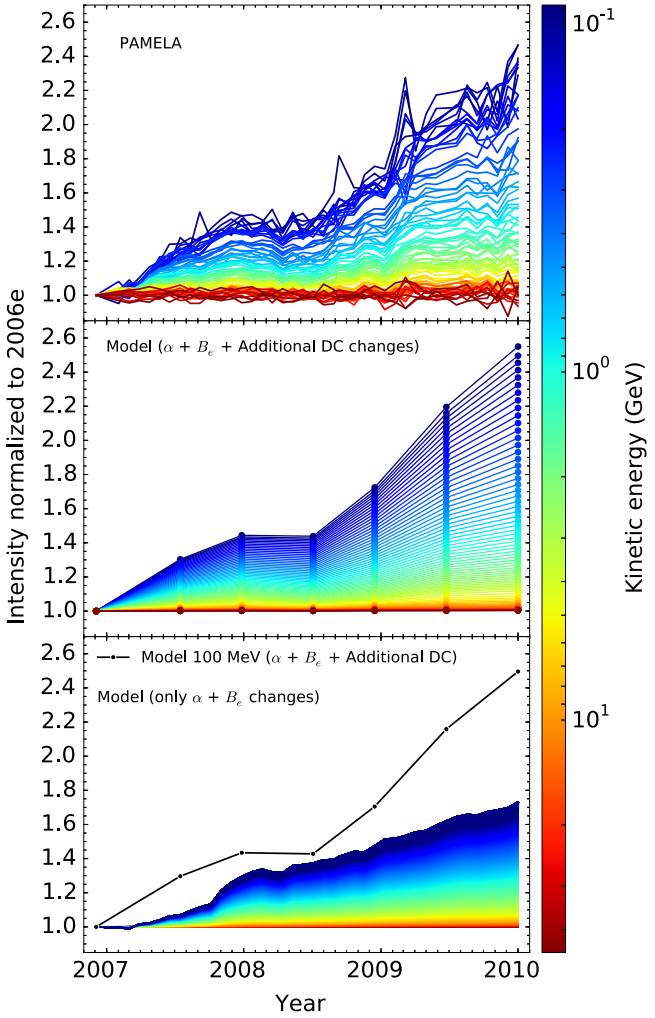

Figure 11. Top panel: *PAMELA* proton intensities between 90 MeV and 50 GeV, normalized to 2006e, as a function of time. Energy values are color coded according to the color bar. Middle panel: similar to the top panel, but for the computed intensities. Changes in α and B_e were considered here, as well as additional DC changes. Bottom panel: similar to the middle panel, but only considering changes in α and B_e. For comparison, the black line represents ~100 MeV computed intensities from the middle panel.

Zhao et al. (2014) similarly studied the *PAMELA* proton spectra between 2007 and 2009, and reported qualitatively similar results, in particular, larger scaling factors for $\lambda_{\perp\, r}$ compared to $\lambda_{\perp\, \theta}$. This suggests a more efficient radial diffusion perpendicular to the background HMF in times of weak turbulence found during solar minima. See also Raath et al. (2015) for a comparison of HMF modifications when reproducing *PAMELA* spectra.

6. SUMMARY AND CONCLUSIONS

With the advent of the 2009 solar minimum, and the availability of 27-day averaged *PAMELA* GCR proton spectra below 50 GeV, we were able to gain insight into how solar modulation affected GCRs during the recent unusual minimum. This was done using a newly constructed proton very LIS based on in situ measurements from *Voyager 1*, *PAMELA*, and *AMS-02*, along with a 3D heliospheric modulation model. After calculating average representative values for the intrinsic parameters α and B_e, seven 27-day averaged *PAMELA* spectra at the end of each semester, between 2006 July and 2009

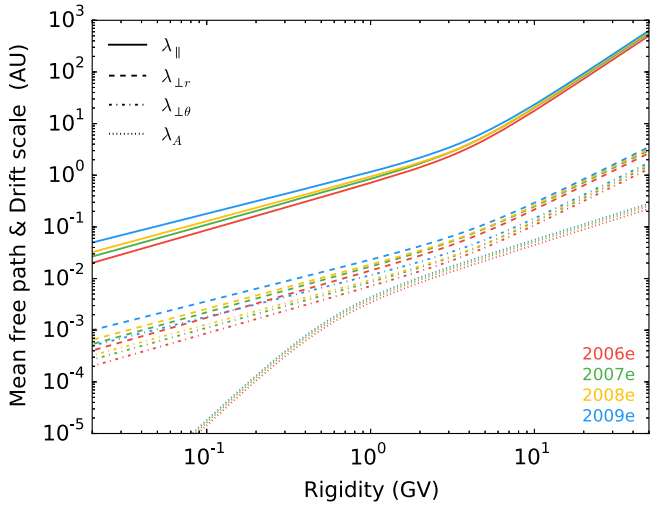

Figure 12. Rigidity dependence of the proton MFPs and drift scale for diffusion parallel and perpendicular to the magnetic field lines at the Earth. Parallel MFPs ($\lambda_\parallel$) are given by the solid lines, while perpendicular MFPs in the radial ($\lambda_{\perp r}$) and polar ($\lambda_{\perp\theta}$) directions are given by the dashed and dashed–dotted lines, respectively. The drift scale (λ_A) is given by the dotted lines. See Equations (3), (8), (9), and (11).

Table 2
Summary of the Parameters Used to Reproduce the Year-end *PAMELA* Spectra

Parameter	2006e	2007e	2008e	2009e
$\lambda_\parallel$ (AU)[a]	0.742	0.888	0.970	1.204
a	0.91	0.88	0.86	0.80
b for $\lambda_\parallel$	2.10	2.10	2.10	2.10
b for $\lambda_\perp$	1.58	1.58	1.58	1.58
c	2.60	2.40	3.0	2.2
P_k (GV)	4.00	4.05	4.08	4.30

Notes. See Equation (5).
[a] MFP values at 1.0 GV at the Earth.

December, were successfully reproduced. It was shown what was required in order for the proton spectrum to become significantly softer as modulation reached extreme minimum levels, increasing intensities by a factor of ∼3 at 100 MeV.

Although the modulation parameters given in Table 2 are different from what was found by Potgieter et al. (2014), primarily due to the differences in the very LIS, the HMF modification, and a different rigidity dependence for perpendicular diffusion, we come here to the same conclusions made by these authors, namely that the rigidity dependence of the DCs had to be decreased over this solar minimum period in order to simulate the *PAMELA* observations. In reproducing these spectra, it was also found that additional increases in proton MFPs below ∼4 GV were required on top of the self-consistent changes in the tilt angle and the weakening HMF strength. It is consequently clear from both observations and modeling that increasingly more low-energy particles reached the Earth during the approximately four years leading up to 2009. Even though diffusion remained a dominant modulation mechanism during this time, the presence of drifts still had a significant contribution to the record-high spectrum measured by *PAMELA* at the peak of the 2009 minimum.

The authors express their gratitude to the South African National Research Foundation (NRF), under the Italy-South African Research Cooperation Programme, for providing partial funding. They also thank the INFN in Italy for partial financial support over several years. Thanks goes to the *PAMELA* group, in particular M. Boezio, V. Di Felice and R. Munini who supplied us with the data, and for many insightful discussions. E.E.V. thanks the South African National Space Agency (SANSA) and NRF for partial financial support during his PhD studies.

REFERENCES

Adriani, O., Barbarino, G. C., Bazilevskaya, G. A., et al. 2013, ApJ, 765, 91
Aguilar, M., Aisa, D., Alpat, B., et al. 2015, PhRvL, 114, 171103
Burger, R. A., Potgieter, M. S., & Heber, B. 2000, JGR, 105, 27447
De Simone, N., Di Felice, V., Gieseler, J., et al. 2011, Ap&SS, 7, 425
Heber, B., & Potgieter, M. S. 2006, SSRv, 127, 117
Hsieh, K. C., Mason, G. M., & Simposon, J. A. 1971, ApJ, 166, 221
Kane, R. P. 2011, SoPh, 269, 451
Luo, X., Zhang, M., Potgieter, M. S., et al. 2015, ApJ, 808, 82
Manuel, R., Ferreira, S. E. S., & Potgieter, M. S. 2014, SoPh, 289, 2207
McComas, D. J., Ebert, R. W., Elliott, H. A., et al. 2008, GeoRL, 35, L18103
Menn, W., Hof, M., Reimer, O., et al. 2000, ApJ, 533, 281
Mewaldt, R. A., Davis, A. J., Lave, K. A., et al. 2010, ApJL, 723, L1
Moraal, H., & Potgieter, M. S. 1982, Ap&SS, 84, 519
Moskalenko, I. V., Strong, A. W., Kunow, H., et al. 2002, ApJ, 565, 280
Ngobeni, M. D., & Potgieter, M. S. 2015, AdSpR, 56, 1525
Parker, E. N. 1965, P&SS, 13, 9
Pei, C., Bieber, J. W., Breech, B., et al. 2010, JGR, 115, A03103
Potgieter, M. S. 2000, JGR, 105, 18295
Potgieter, M. S. 2013, LRSP, 10, 3
Potgieter, M. S., Vos, E. E., Boezio, M., et al. 2014, SoPh, 289, 391
Potgieter, M. S., Vos, E. E., Munini, R., et al. 2015, ApJ, 810, 141
Raath, J. L., Potgieter, M. S., Strauss, R. D., & Kopp, A. 2015, arXiv:1506.07305
Richardson, J. D., & Wang, C. 2011, ApJL, 734, L21
Shalchi, A. 2009, ASSL, Vol. 362 (Berlin: Springer)
Shikaze, Y., Haino, S., & Abe, K. 2007, APh, 28, 154
Smith, C. W., & Bieber, J. W. 1991, ApJ, 370, 435
Stone, E. C., Cummings, A. C., McDonald, F. B., et al. 2013, Sci, 341, 150
Strauss, R. D., & Potgieter, M. S. 2014a, AdSpR, 53, 1015
Strauss, R. D., & Potgieter, M. S. 2014b, SoPh, 289, 3197
Strauss, R. D., Potgieter, M. S., Ferreira, S. E. S., et al. 2013, ApJL, 765, L18
Von Rosenvinge, T. T., McDonald, F. B., Trainor, J. H., et al. 1979, Proc. ICRC, 12, 171
Webber, W. R., Golden, R. L., Stochaj, S. J., et al. 1991, ApJ, 380, 230
Webber, W. R., & McDonald, F. B. 2013, GeoRL, 40, 1665
Zhao, L. L., Qin, G., Zhang, M., et al. 2014, JGR, 119, 1493